sustainability

MDPI

Article

Quantifying the Impacts of Climate Change on Streamflow Dynamics of Two Major Rivers of the Northern Lake Erie Basin in Canada

Binbin Zhang, Narayan Kumar Shrestha, Prasad Daggupati *, Ramesh Rudra, Rituraj Shukla, Baljeet Kaur and Jun Hou

School of Engineering, University of Guelph, 50 Stone Rd E, Guelph, ON N1G 2W1, Canada; binbin@uoguelph.ca (B.Z.); shresthn@uoguelph.ca (N.K.S.); rrudra@uoguelph.ca (R.R.); rshukla@uoguelph.ca (R.S.); baljeet@uoguelph.ca (B.K.); jhou02@uoguelph.ca (J.H.)
* Correspondence: pdaggupa@uoguelph.ca; Tel.: +519-760-9299

Received: 1 May 2018; Accepted: 10 August 2018; Published: 15 August 2018

Abstract: This paper focuses on understanding the effects of projected climate change on streamflow dynamics of the Grand and Thames rivers of the Northern Lake Erie (NLE) basin. A soil water assessment tool (SWAT) model is developed, calibrated, and validated in a base-period. The model is able to simulate the monthly streamflow dynamics with 'Good' to 'Very Good' accuracy. The calibrated and validated model is then subjected with daily bias-corrected future climatic data from the Canadian Regional Climate Model (CanRCM4). Five bias-correction methods and their 12 combinations were evaluated using the Climate Model data for hydrologic modeling (CMhyd). Distribution mapping (DM) performed the best and was used for further analysis. Two future time-periods and two IPCC AR5 representative concentration pathways (RCPs) are considered. Results showed marked temporal and spatial variability in precipitation (−37% to +63%) and temperature (−3 °C to +14 °C) changes, which are reflected in evapotranspiration (−52% to +412%) and soil water storage (−60% to +12%) changes, resulting in heterogeneity in streamflow (−77% to +170%) changes. On average, increases in winter (+11%), and decreases in spring (–33%), summer (−23%), and autumn (−15%) streamflow are expected in future. This is the first work of this kind in the NLE and such marked variability in water resources availability poses considerable challenges to water resources planners and managers.

Keywords: climate change; bias-correction; Northern Lake Erie basin; streamflow; SWAT

1. Introduction

The Great Lakes, bordering Canada and the United States of America (USA), provide fresh water resources for consumption, transportation, tourism, and power generation, among others, to the surrounding inhabitants, communities, and industries, thereby contributing significantly to the environment and economy. Lake Erie—the southernmost and the shallowest of the five lakes is home to approximately 14 million people [1]. In the last few decades, serious blue-green algae blooms have been observed in the Lake. As a result of the Great Lakes Water Quality Agreement (GLWQA) between Government of Canada and USA in 1972, marked reduction of phosphorus load helped to improve the water quality of the lake significantly [2]. However, in recent times, the algae bloom resurfaced again mainly due to the increased levels of harmful pollutants and phosphorous primarily from agricultural lands within the Lake Erie basin [3]. For instance, in 2011, Lake Erie experienced the largest harmful algal bloom in its historical record, which was estimated to be at least 2.4 times higher than any previous records [4]. Various 'economic, management, climatic, and political' factors

and their complex interrelations are responsible for the algae blooms [5], which have affected various sectors and the economy. In light of growing evidence of climatic change, such as significant increases in winter temperature [6], decreases in snowfall proportion on total precipitation [7], changes in lake level [8], changes in streamflow input to the lake [9], changes in freeze-thaw frequencies [6], increases in drought and flood frequency [7], changes in ice cover [9], among others in the Great Lakes area, it is of paramount importance that climate change impact assessments on different hydrologic and water quality components are carried out, and plausible adaptation measures are undertaken immediately. As hydrology is one of the main drivers of pollutants [10], quantification of climate-induced altercation on different water resources components and on streamflow dynamics is required in the first place.

Currently, there are many studies which have evaluated the effect of climate change on the streamflow delivery to Lake Erie, but these studies are mainly situated in basins that lie on the USA side. For instance, Bosch et al. [11] reported annual stream streamflow increases of 6–12% in the future (2010–2099) from the Western and the Central Lake Erie basin for different emission scenarios (SRES A1F1 and B1) using 3 Global Circulation Models (GCMs); US National Atmospheric and Oceanic Administration's Geophysical Fluid Dynamics Laboratory (GFDL) CM2.1, UK Meteorological Office's Hadley Center Climate Model V3 (HadCM3), and US National Center for Atmospheric Research's Parallel Climate Model (PCM). Similarly, Culbertson et al. [12] reported that annual streamflow increased by 6.5–15.9% using an ensemble of 15 GCMs (refer to Culbertson et al. [12] for the full list) in the Maumee River basin, the largest basin in Western Lake Erie in different emission scenarios (RCP 4.5 and RCP 8.5), and during different future periods (2010–2039, 2040–2069, 2070–2099). Furthermore, Verma et al. [13] predicted an annual increase of 9.7% in the same river basin. In contrast, very few climate change impact studies are conducted in the basins draining from the Canadian side. In a recent study, Li et al. [14] reported, using Proving Regional Climate for Impact Studies (PRECIs) data, decreases in summer streamflow and increases in winter streamflow during 2071–2100 for SRES A2 and B2 in the Grand River basin, the largest basin of Northern Lake Erie. However, to our knowledge, there has not been a single study which evaluated climate change impacts on streamflow of the entire Northern Lake Erie basin. Hence, in this study, we have considered two major river basins—the Grand and the Thames of Northern Lake Erie, which drain almost 60% of the total basin area.

It is in this scope that we built up, calibrated and validated a hydrological model of the Northern Lake Erie basin using the Soil and Water Assessment Tool (SWAT) [15] using a high-resolution spatial and meteorological dataset. The calibrated and validated model in the base period (1980–1993) was then subjected to bias-corrected high-resolution (25 km $\times$ 25 km) future climate data of a regional circulation model: the Canadian Regional Climate Model (CanRCM4) [16] to quantify streamflow dynamics in the future. As such, we used the Climate Model data for the hydrologic modeling (CMhyd) tool [17], and evaluated five bias-correction methods for precipitation and temperature. Moreover, we considered two IPCC emission scenarios—RCP4.5 & RCP8.5 [18] and two future periods: mid-(2040–2053) and end-century (2080–2093). We believe that the availability of such a modelling tool, and we know how the climate-induced hydrological altercations could be helpful to understand the distribution and availability of water resources in the future, and would help in formulating plausible management options with the view of mitigating any ill effects on the health of Lake Erie.

2. Materials and Methods

2.1. Study Area

The Northern Lake Erie (NLE) basin is located at Southwestern Ontario region of Canada and has approximately 21750 km^2 of drainage area. The Grand and Thames river basins are the two largest sub-basins (Figure 1), comprising areas of 6764 and 5883 km^2, respectively. Agriculture is the dominant land-use in both river basins (44% and 69% coverage, respectively, for the Grand and Thames river basins), followed by pasture (25% and 11%, respectively), forest (17% and 10%, respectively) and urban (9% and 8%, respectively). (Figure S1). The general weather pattern is cold with dry winters, due to

the effect of Arctic air from the Northwest, and warm and wet summers due to the tropical air masses from Gulf of Mexico. However, the basin experiences rather uniform precipitation. Annual mean precipitation, as calculated using Gridded Climate Dataset for Canada (GCDC) [19] for the period of 1980–1993 varied between 833 and 1000 mm. The amount of precipitation in the central part of the basin is slightly higher than that in the west and east basin. As the basin lies in a cold climate region, snowstorms in the winter and snowmelt in the spring is typical in the study area, which results in high streamflow in the early spring months, March and April. Similarly, annual mean temperature varies from 5.1 °C in the high elevation area to 9.7 °C in the low elevation area [19].

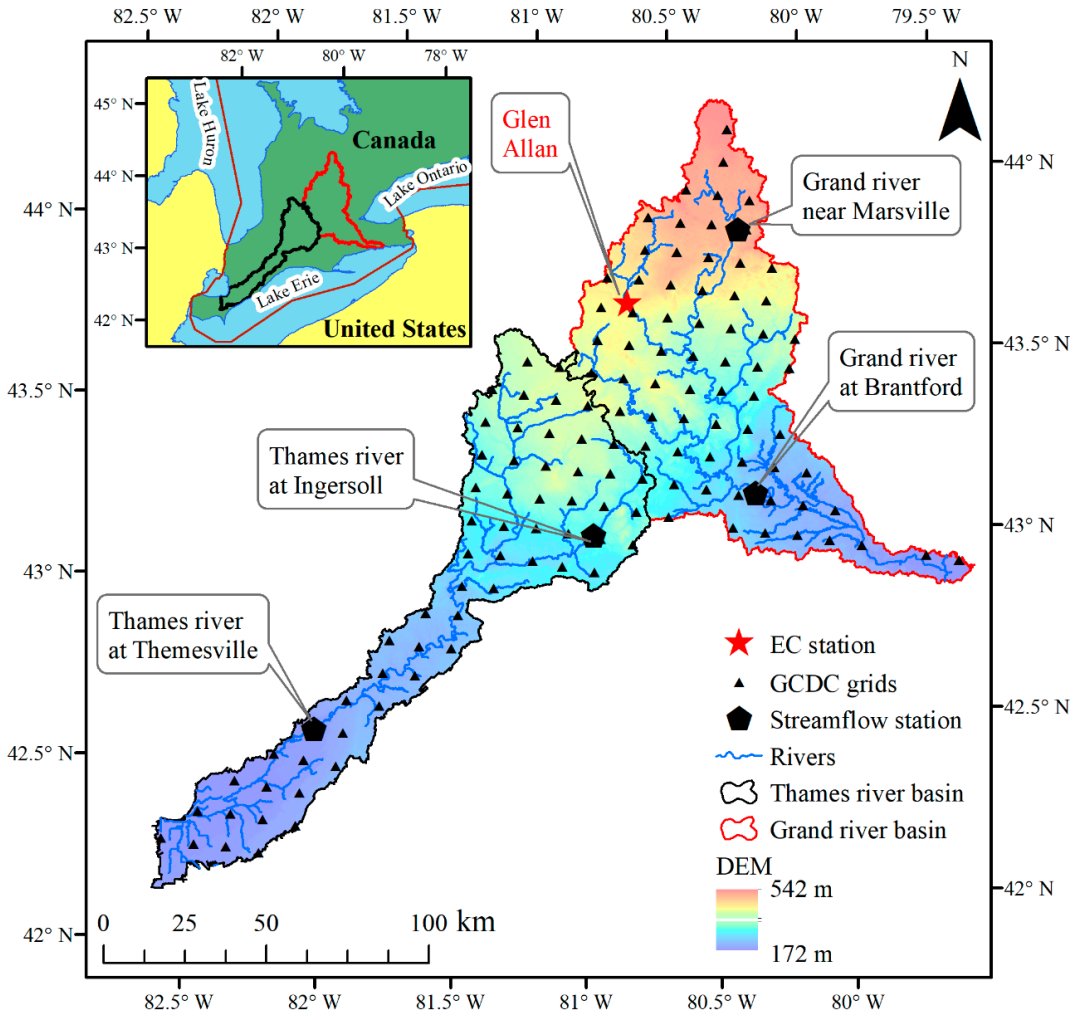

Figure 1. The Great Lakes (inset) with two major river basins—the Grand and the Thames of the Northern Lake Erie Basin. Also shown are a digital elevation model (DEM), a generated river network, four streamflow gauging stations (pentagons), the grid-centroid location of the Gridded Climate Dataset for Canada (GCDC) stations (triangles), and an Environmental Canada (EC) station (Glen Allan) used for bias-correction of future precipitation and temperature datasets.

The basin is drained by two main rivers—the Grand and the Thames rivers within the NLE basin. The Grand River basin is the largest watershed in Southwestern Ontario, with a drainage area of almost 6800 km^2. The length of the Grand River is about 300 km from the upper stream near the town Dundalk, to the mouth of the river on the Lake Erie [20]. The elevation ranges from 172 m to 539 m. Most of the area is flat, with the slope ranging from 0 to 4% (Figure S3). The Grand River watershed drains a high-density populated area with five growing cities in its catchment—Kitchener, Waterloo, Cambridge, Guelph, and Brantford, which is a unique feature of the rivers in the region. The watershed

is home to approximately 1 million people, which is expected to increase to over 1.4 million by 2031 [21]. Therefore, the effects of human activity on river hydrology and morphology in the Grand River basin is expected to be significant in the future. The Thames River basin, on the other hand, is the second largest watershed in Southwestern Ontario, with a catchment area of 5880 km^2. It flows approximately 273 km from the upper stream near Tavistock to its mouth at Lake St. Clair. The Upper Thames River Basin (UTRB) is one of the highly developed areas in the entire basin with a population of 460,000 [22]. Prodanovic and Simonovic [23] reported that UTRB has had well-documented flooding events since 1700s, and experiences frequent drought spells. Thus, in the light of growing evidences of climate change, it is evident that the basin would face extra pressure of the climate, demographic, and anthropogenic changes in the future.

2.2. The Model—Soil and Water Assessment Tool (SWAT)

The SWAT is a continuous-time, semi-distributed, and physically-based watershed-scale model, which integrates weather, land-use, soil type, surface, and groundwater hydrology to simulate streamflow, sediment, water quality, etc. within a watershed [15,24]. It is one of the most widely used hydrological simulators around the world, including the cold climate regions of Canada after careful parametrization [25–31]. The model divides a watershed into various sub-watersheds. The sub-watersheds are further divided into Hydrologic Response Units (HRUs), which are unique combination of land-use, soil and slope. The SWAT requires different spatial and meteorological datasets, generally integrated using geographic information system (GIS) software [32].

2.3. Model Build-Up, Inputs, Calibration and Validation

We used a 30 mx30 m digital elevation map (DEM, Figure 1) obtained from the Ontario Ministry of Natural Resources and Forestry [33]. The DEM was then used to delineate the watershed boundary and streams. Furthermore, the DEM was used to derive two slope classes: 0–4%, and >4% (Figure S3), which were later used to set up the model. Land use data encompassing the watershed was generated from 2015 and 2016 spatial crop data layers (CDL) from the Agriculture and Agri-Food Canada (AAFC) annual crop inventory. In this study, several post-processing techniques were used to combine CDL and spatial agricultural tile drainage maps (OMAFRA) to prepare a land use/land cover map at a 30 m resolution that had crop rotations and tile drainage included (Figure S1). Soil data at a scale of 1:1 million (Figure S2) obtained from Soil Landscapes of Canada (SLC) version 3.2 was used. Threshold values of 10%, 5%, and 5% for land-use, soil and slope, respectively, were used to define the HRUs. These processes resulted in a total of 7539 HRUs and 244 sub-basins in the SWAT model of the study area. Moreover, a 10 km $\times$ 10 km gridded GCDC precipitation, and maximum and minimum temperature data [19] (Figure 1) obtained from AAFC at daily time interval for a period of 1980–1993 were used. This GCDC data was interpolated from daily Environment Canada climate station observations using a thin plate smoothing spline surface fitting method [19]. The model was run for a period 1980–1993, of which the first three years were used as a warm-up period.

2.4. Model Performance Evaluation

We followed the recommendation of Moriasi et al. [34] to evaluate the SWAT model performance in simulating streamflow in the base period (1983–1993, 1983–1988—the calibration period, and 1989–1993—the validation period). As such, we considered three goodness-of-fit statistics, the coefficient of determination (R^2), the Nash-Sutcliffe efficiency (NSE) [35], and the percentage of bias (PBIAS), and the range of values of these statistics, for a particular qualitative rating (very good, good, satisfactory, and unsatisfactory). In case different goodness-of-fit statistics pointed to different qualitative ratings, an average qualitative rating was calculated, as adopted by various studies [36,37]. In addition, different graphical plots (e.g., time series, scatter plots, etc.) were also used. We used daily streamflow measurements (averaged to monthly) at four gauging stations (Figure 1, two each for the Thames and Grand river basins) for this purpose.

2.5. Future Climate Data

While numerous climate change projection data exist, we used future climatic data (precipitation, and minimum and maximum temperatures) from a Canadian regional climate model, the CanRCM4, to quantify the impacts on streamflow dynamics. The projections from the CanRCM4 are tailored to applications in Canada and are one of the RCMs used in the Coordinated Regional Climate Downscaling Experiment (CORDEX) project implemented by the World Climate Research Programme (WCRP) [16]. The CanRCM4 was developed using a dynamic method with a parent driver, which is a second generation Canadian Earth System Model (CanESM2, readers are referred to Scinocca et al., von Salzen et al. [16,38] for further details). The spatial resolution of the CanRCM4's horizontal grid of 0.22° was equivalent to 25 km. Two emission scenarios, the Representative Concentration Pathway (RCP) 8.5 and 4.5, as purposed in the Fifth Assessment Report (AR5) by Intergovernmental Panel on Climate Change (IPCC) [18], were used in this study. The RCP8.5 is a high emission scenario representing an equivalent concentration of CO_2 larger than 1000 ppm in 2100, while RCP4.5 is an intermediate emission scenario with an equivalent concentration of CO_2 ranging from 580 to 720 ppm in 2100 [18]. Furthermore, two future periods—a mid- (2043–2053) and an end-century (2083–2093) period were used to assess the impacts. We believe that the inclusion of two emission scenarios and two future periods will reduce the uncertainties as advocated by Hawkins and Sutton [39]. However, it should be noted that use of additional climate projection data might be helpful in understanding the variability in projected streamflow. A study by Cheng et al. [40] in a similar cold climate region watershed of western Canada using 6 CMIP5 GCMs showed that the ensemble mean projections could not outperform any GCMs, indicating that the use of a suitable GCM might be enough. However, choosing an appropriate GCM/RCM after a systematic evaluation of multiple climate models should always be a preferred option. As such, it should be noted that the parent GCM of the CanRCM4 was indeed one of the top 3 best performing models for this region of Canada [41].

2.6. Bias-Correction Methods

This study used the Climate Model data for hydrologic modeling (CMhyd) [17], which can be used both for extracting and bias-correcting climate variables that are obtained from GCMs and RCMs. The CMhyd is tailor-made to prepare simulated climate variables for climate change impact studies with the SWAT model. The tool offers several bias-correction methods, including linear scaling, non-linear scaling, and distribution mapping. Readers are referred to Rathjens et al. [17] for further details about the tool. These bias-correction methods are explained briefly hereafter.

Since the performance of bias-correction methods is stationary between different weather stations [42], one real-time Environmental Canada weather station—the Glen Allan (Figure 1) was chosen as a reference station to evaluate the following bias-correction methods. The annual mean precipitation at the station, calculated using daily data during the period of 1964–1993, was 961.2 mm. Similarly, the mean summer precipitation was 254.7 mm—slightly higher than the winter mean (216.8 mm). Moreover, the mean annual temperature was 6.6 °C, calculated using the same time frame. To further evaluate the bias-correction methods, GCDC stations (Figure 1) were also used. This served as a proxy-validation of the improvements achieved through each of the following bias-correction methods.

2.6.1. Linear Scaling (LS) of Precipitation and Temperature

For the precipitation time series, a ratio was defined as the quotient of the long-term mean of the observed monthly precipitation to that of the RCM simulations. The ratio was then used to multiply the simulated daily precipitation of the corresponding month [43].

$$P_{con,cor(d)} = P_{con(d)} \times \left(\frac{\overline{P_{obs(m)}}}{\overline{P_{con(m)}}} \right) \quad (1)$$

$$P_{sec,cor(d)} = P_{sec(d)} \times \left(\frac{\overline{P_{obs(m)}}}{\overline{P_{con(m)}}} \right) \quad (2)$$

where, $P_{con,cor(d)}$ is the corrected daily precipitation in the corresponding month during the control period; $P_{sec,cor(d)}$ is the same during the future period; $P_{con(d)}$ is the uncorrected daily precipitation in the corresponding month during the control period; $P_{sec(d)}$ is the same during the future period; $\overline{P_{obs(m)}}$ is the observed monthly mean precipitation in the corresponding month during the control period; $\overline{P_{con(m)}}$ is the simulated monthly mean precipitation in the corresponding month during the future period.

For temperature time series, however, an additive term is was defined as the difference between the long-term mean of the observed monthly temperature, and that of the RCM simulations. The additive term was then added to the simulated daily temperature of the corresponding month [43].

$$T_{con,cor(d)} = T_{con(d)} + \left(\overline{T_{obs(m)}} - \overline{T_{con(m)}} \right) \quad (3)$$

$$T_{sec,cor(d)} = T_{sec(d)} + \left(\overline{T_{obs(m)}} - \overline{T_{con(m)}} \right) \quad (4)$$

where, $T_{con,cor(d)}$ is the corrected daily temperature in the corresponding month during the control period; $T_{sec,cor(d)}$ is the same during the future period; $T_{con(d)}$ is the raw daily temperature in the corresponding month during the control period; $T_{sec(d)}$ is the same during the future period; $\overline{T_{obs(m)}}$ is the observed monthly mean temperature in the corresponding month during the control period; $\overline{T_{con(m)}}$ is the simulated monthly mean temperature in the corresponding month during the future period.

2.6.2. Local Intensity Scaling (LOCI) of Precipitation

It is widely reported that RCM simulations tend to overestimate the numbers of drizzle days, and wet-days frequency of the RCM simulated precipitation time series would be larger than that of the observed precipitation [44,45]. As the LS method can only adjust the mean, the LOCI method was thus developed, using a wet-days threshold to further adjust the wet-days frequencies [46]. In this method, three steps were generally defined. First, the wet-days threshold was determined so that numbers of days, excluding the days when precipitation was smaller than a chosen threshold value in the RCM simulations, was the same as that of the observed wet-days when precipitation exceeded 0 mm. The governing equations of the LOCI method are [47]:

$$P^1_{con,(d)} = \begin{cases} 0, & if\ P_{con,(d)} < P_{thres} \\ P_{con,(d)}, & otherwise \end{cases} \quad (5)$$

$$P^1_{sec,(d)} = \begin{cases} 0, & if\ P_{sec,(d)} < P_{thres} \\ P_{sec,(d)}, & otherwise \end{cases} \quad (6)$$

where $P^1_{con,(d)}$ is the transitional daily precipitation during the control period; $P^1_{sec,(d)}$ is the same during the future period; $P_{con,(d)}$ is the original daily precipitation during the control period; $P_{sec,(d)}$ is the same during the future period; P_{thres} is the threshold.

Secondly, a scaling factor was calculated as a ratio of wet-day intensity between the observed precipitation time series and the RCM simulations, and later adjusted using the adopted precipitation threshold [46]:

$$s = \frac{\mu(P_{obs,m,d}/P_{obs,m,d} > 0) - 0}{\mu(P_{con,m,d}/P_{con,m,d} > P_{thres}) - P_{thres}} \quad (7)$$

Finally, the corrected daily precipitation was computed using a scaling factor multiplied by transition daily precipitation:

$$P_{con,cor(d)} = s \times P^1_{con,(d)} \tag{8}$$

$$P_{sec,cor(d)} = s \times P^1_{sec,(d)} \tag{9}$$

where $P_{con,cor(d)}$ is the corrected daily precipitation during the control period; $P_{sec,cor(d)}$ is the same during the future period; s and $P^1_{sec,(d)}$ is the same in Equations (5)–(7).

2.6.3. Power Transformation (PT) of precipitation

It is widely accepted that the LS and LOCI methods cannot adjust biases in the variance [47]. Hence, a non-linear method, also referred to as the power transformation (PT), which uses an exponential form of $P^* = \mathrm{a}P^{b_m}$ to further adjust the standard deviation of RCM simulations [48,49], was also tested. As such, two steps were generally followed. Firstly, a scaling factor, b_m, was calculated to ensure that the coefficient of variance of RCM was the same as that of the observations on a monthly basis [47]:

$$\mathrm{f}(b_m) = 0 = CV_m(P_{obs}(d)) - CV_m\left(P^{b_m}_{con}(d)\right) \tag{10}$$

Next, the same procedure as the LS method was applied to $P^{b_m}_{con}(d)$ and $P^{b_m}_{sce}(d)$ such that the monthly mean precipitation was the same between RCM simulated and observed precipitation time series.

2.6.4. Variance Scaling (VS) of temperature

While PT is an effective way to correct both mean and variance of precipitation time series, the method, however, cannot be used to adjust the variance of the temperature time series, since the temperature is normally distributed [50]. Therefore, another method—the variance scaling (VS), was applied to bias-correct the temperature time series [47], and is given as [48]:

$$T_{cor,m,d} = [T_{con,m,d} - \mu(T_{con,m})] \times \frac{\sigma(T_{obs,m})}{\sigma(T_{con,m})} + \mu(T_{obs,m}) \tag{11}$$

where $T_{cor,m,d}$ is the corrected daily temperature; $T_{con,m,d}$ is the uncorrected daily temperature in the corresponding month during the control period; $\sigma(T_{obs,m})$ is the standard deviation of the observed temperature time series in the corresponding month; $\sigma(T_{con,m})$ is the standard deviation of RCM temperature time series in the corresponding month; $\mu(T_{obs,m})$ is the observed monthly mean temperature in the corresponding month.

2.6.5. Distribution Mapping (DM) for Precipitation and Temperature

Distribution mapping (DM), also referred to as histogram equalization, quantile-quantile mapping, or probability mapping, is a popular bias-correction method used in numerous climate change studies [44,45,51,52]. The basic principle was to fit the parameters of transfer functions of RCM-simulated data to that of observed data based on the monthly mean value. Typically, two transfer functions are suitable for describing climate data: the Gamma and Gaussian distributions for precipitation and temperature, respectively. For precipitation, firstly, random precipitation intensity was specified and was used to determine the cumulative probability of simulated precipitation. Then, based on the cumulative probability, the corrected precipitation value is selected. For temperature, the cumulative probability of simulated temperature data could be determined. Then, according to the probability, the corrected temperature value can be selected.

2.7. Evaluation of Bias-Correction Methods

As depicted already, different bias-correction methods for precipitation and temperature would be used. The performance of each bias-correction methods would be evaluated using frequency—as well as time-series-based statistics. As such, we used mean, median, standard deviation, coefficient-of-variation, and 90th percentile as frequency-based statistics for both precipitation and temperature. Moreover, probability and intensity of wet-days were considered for precipitation. Furthermore, we used four time-series-based statistics, R^2, PBIAS, NSE, and mean absolute error (MAE). Finally, monthly time series plots were analyzed in order to evaluate temporal patterns of bias-corrected precipitation and the temperature CanRCM4 dataset.

Furthermore, it is widely reported that a bias-correction method that performs well in the historical case is expected to perform better for the future scenarios [47]. It thus becomes imperative to assess the accuracy of streamflow dynamics using all bias-corrected CanRCM4 datasets, and to compare them with streamflow simulations using the observations and with those simulated using the raw dataset. This would further refine our search for the best performing bias-correction method during the base period, which would then be used for further analysis in the future periods. As such, 12 different combinations were defined and simulated with the SWAT model to assess streamflow dynamics in the base period. In order to compare the performance of the different bias-correction methods on streamflow simulations, baseline streamflow simulations were used as the reference simulations at four streamflow gauging stations, two each for the Grand and Thames river basins (Figure 1). The performance of different combinations of bias-correction methods on streamflow was evaluated using three time-series-based goodness-of-fit statistics (R^2, PBIAS and NSE).

3. Results and Discussion

3.1. Streamflow Results in the Base Period

Figure 2 shows a graphical comparison of observed and simulated monthly streamflow during the calibration as well as the validation period at four stations, two each for the Grand River and the Thames River. Similarly, the goodness-of-fit statistics of the model results are presented in Table 1. In general, there is a significant correlation between simulated and observed streamflow in both of the watersheds. Similarly, the simulated streamflow also followed the trend of the observations. During the calibration period, in the Grand River, the PBIAS value ranged from −10% to −2% from the upper watershed location to the downstream location, NSE value ranged from 0.78 to 0.77, and R^2 values ranged from 0.8 to 0.88. The qualitative ratings, as calculated from the range of values of these goodness-of-fit statistics recommended by Moriasi et al. [34], ranged from 'Satisfactory' to 'Very Good'. On average, the qualitative ratings at both upstream and downstream stations are calculated to be 'Good'. In the Thames River, the PBIAS ranged from 7% to 1%, the NSE ranged from 0.84 to 0.91, and the R^2 ranged from 0.85 to 0.9 from the upper watershed location to the downstream location. As per the calculated goodness-of-fit statistics, the model performance in the calibration period varied from 'Good' to 'Very Good'. On average, the qualitative ratings were 'Very Good' at both stations in the Thames River basin. In general, the model performances during the validation period were found to be similar, when compared with that of the calibration period. Our model results were comparable to the reported statistics in similar cold climate regions of Canada [25–31].

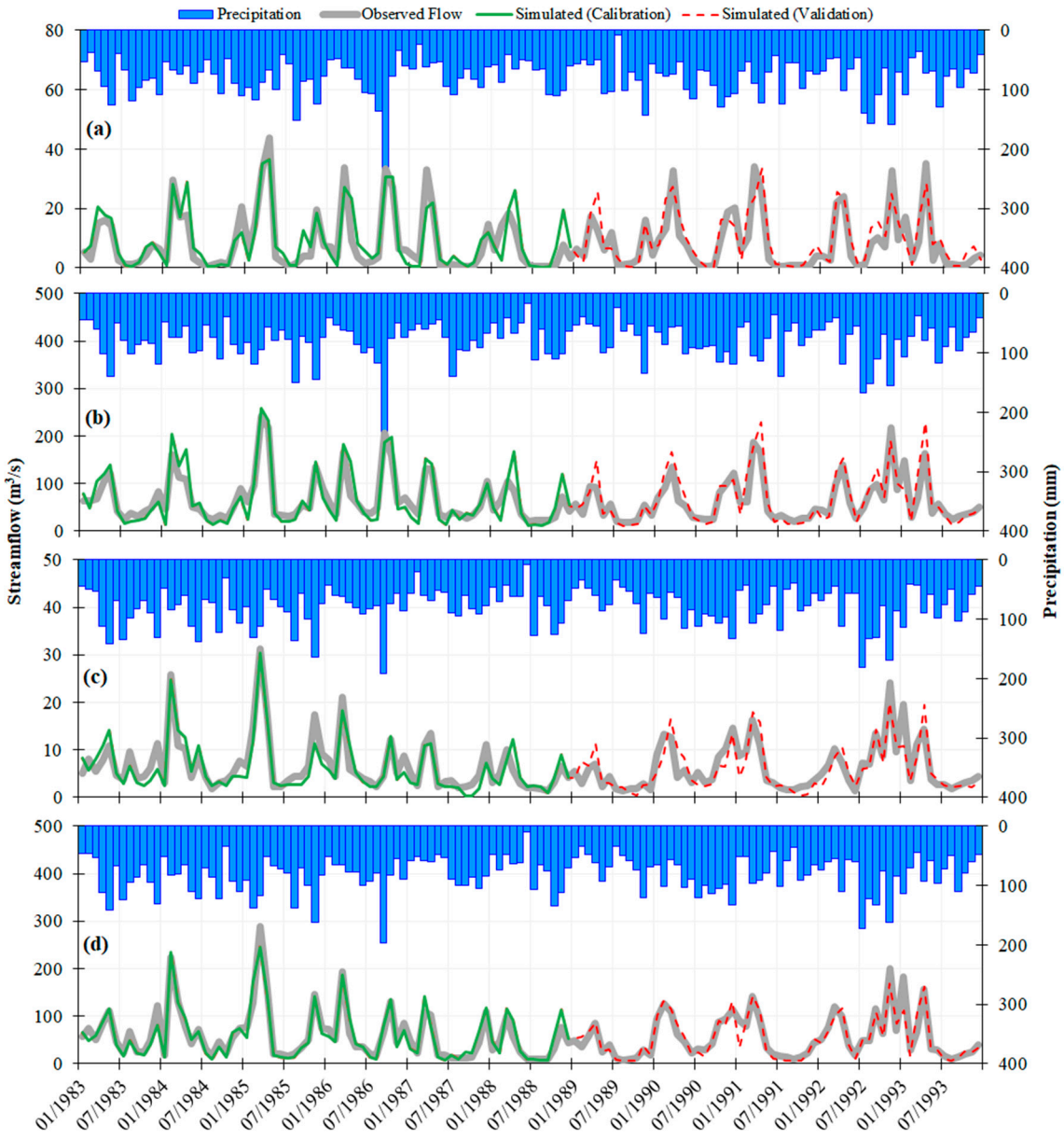

Figure 2. Time series plots of observed and simulated monthly streamflow at: (**a**) Grand River near Marsville (**b**) Grand River at Brantford (**c**) Thames River at Ingersoll (**d**) Thames River at Thamesville during both calibration and validation periods. Also shown is the precipitation time series as inverted bars.

Table 1. Goodness-of-fit statistics and qualitative ratings of streamflow simulation results during both calibration and validation periods at four stations.

Streamflow Gauging Stations	Calibration			Validation		
	R^2	PBIAS (%)	NSE	R^2	PBIAS (%)	NSE
Grand river near Marsville	0.80(G)	–10(S)	0.78(G)	0.77(G)	–14(S)	0.74(G)
Grand river at Brantford	0.88(VG)	–2(VG)	0.77(G)	0.83(G)	–7(G)	0.72(G)
Thames river at Ingersoll	0.85(VG)	7(G)	0.84(VG)	0.75(G)	5(G)	0.73(G)
Thames river at Thamesville	0.91(VG)	1(VG)	0.91(VG)	0.88(VG)	3(VG)	0.88(VG)
VG: Very Good; G: Good; S: Satisfactory; US: Unsatisfactory						
R^2: Coefficient of determination; PBIAS: Percentage of bias; NSE: Nash-Sutcliffe Efficiency						

3.2. Performance of Different Bias-Correction Methods

3.2.1. Precipitation

Four bias-corrected methods used in this study significantly improved simulated precipitation time series as indicated by goodness-of-fit statistics of both frequency- and time-series-based statistics (Table 2). Figure 3 shows the graphical comparison plots of these statistics calculated for the observed, raw and bias-corrected daily precipitation data.

Table 2. Frequency- (daily) and time-series- (monthly) based statistics for the precipitation of observed, raw CanRCM4, and bias-corrected (using four methods) CanRCM4 datasets during a period of 1964–1993.

Statistics	Obs.	Raw	LS	LOCI	PT	DM
Frequency based						
Mean (mm)	2.71	2.39	2.71	2.71	2.71	2.69
Median (mm)	0	0.21	0.24	0	0.39	0
Standard Deviation (mm)	6.14	6.1	7.14	7.26	6.14	7.28
Coefficient of Variation (-)	2.26	2.55	2.63	2.68	2.26	2.7
90th Percentile (mm)	8.6	6.89	7.57	7.69	7.81	7.5
Probability of Wet Days (%)	47.12	81.1	81.1	46.89	81.1	46.89
Intensity of Wet Days (mm/day)	5.76	2.95	3.34	5.79	3.34	5.75
Time-series based						
Coefficient of Determination - R^2	-	0.04	1	1	1	0.99
Percentage Bias - PBIAS (%)	-	11.8	0.01	0	0	0.69
Nash-Sutcliffe Efficiency - NSE	-	–0.7	1	1	1	0.99
Mean Absolute Error - MAE (°C)	-	16.92	0.01	0	0.01	1.08
LS: Linear Scaling; LOCI: Local Internsity Scaling; DM: Distribution Mapping						

Raw CanRCM4 data seriously underestimated the mean precipitation for the months of August to October, compared to that of the observations, resulting in an overall underestimation (2.39 mm compared to 2.71 mm). However, all the bias-correction methods effectively reduced the discrepancy. No significant differences on performance between four bias-correcting methods were found. As for the standard deviation (SD), the raw data again showed marked temporal heterogeneity (Figure 3). Compared to that of the observations (6.14 mm), the SDs for the months of January to June, calculated using the raw CanRCM4 data were overestimated, while they were underestimated in the following months, resulting in an overall SD value of 6.1 mm. After bias-correction, significant improvements in the temporal trend of the SDs were evident (Figure 3). While the PT method perfectly adjusted the SD, the other three methods tended to over-adjust the SDs, especially for the months of April and December. Similarly, the raw dataset tends to overestimate the coefficient-of-variation (CV) for most of the months,

except for March. The LS-, LOCI-, and DM-based bias-correction methods were found to be poor to adjust CV, as the resulting CVs were found to be 2.63, 2.68, and 2.7, respectively, which were seriously overestimated compared to the observed value of 2.26. In contrast, the PT method was found to be the best method in adjusting the biases in CV with zero overall bias. Moreover, the biases on 90th percentile precipitation for the raw CanRCM4 dataset were apparent in different months (Figure 3), resulting in an overall underestimation (6.89 mm), compared to the observations (8.6 mm). After applying bias-correction methods, all methods significantly reduced biases, but the extent of improvements were fairly comparable (7.5–7.81 mm, compared to 8.6 mm for the observations). Furthermore, the raw CanRCM4 dataset significantly overestimated the probability of wet-days (81.1%), compared to the observations (47.12%) as did the LS and PT methods (81.1%). The LOCI and DM methods, on the other hand, improved both the temporal trend and the overall statistics of the probability of wet-days significantly (46.89% for both methods, compared to 47.12% for the observations). Finally, the raw CanRCM4 dataset significantly underestimated the intensity of wet-days in all months, resulting in a significant overall underestimation (2.95 mm/day compared to 5.76 mm/day for the observations) which was contrary to the trend that was observed for the wet-days frequency. After applying bias-correction methods, similar results to the observed probability of wet-days were obtained (better performance of LOCI and DM methods compared to the LS and PT methods).

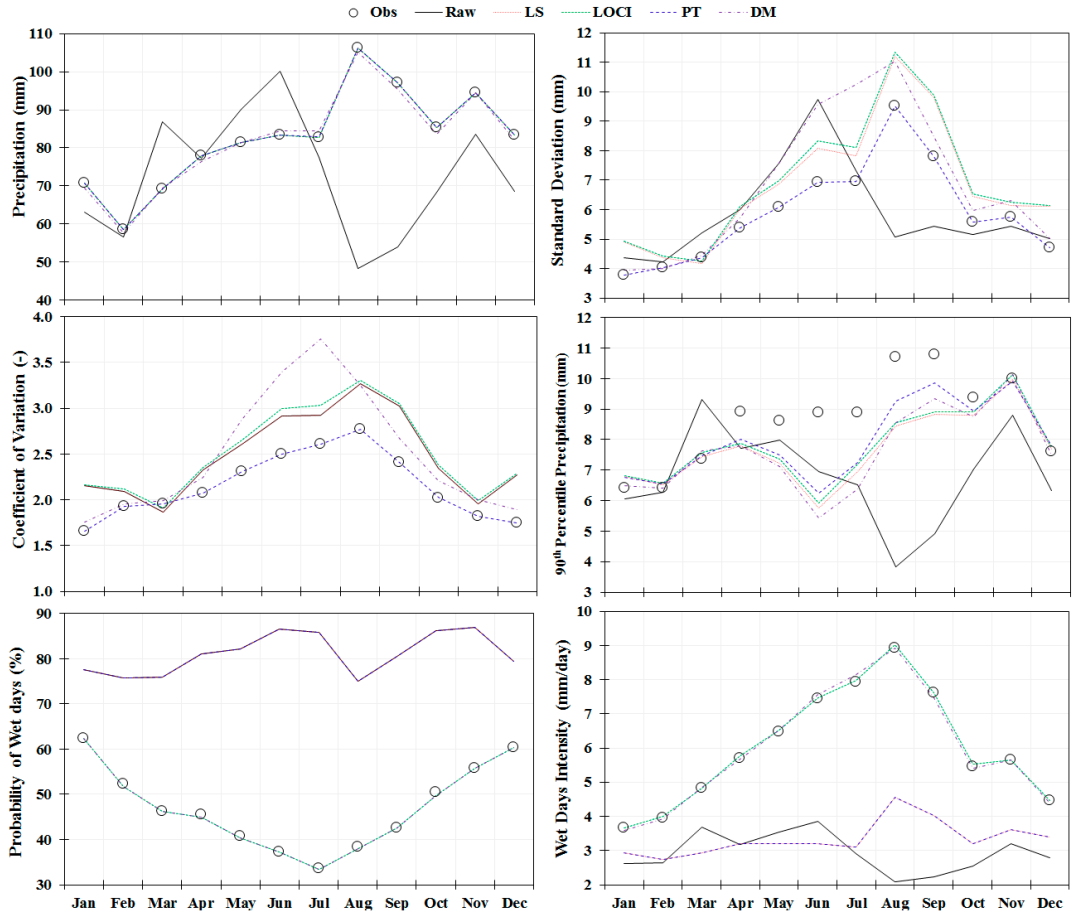

Figure 3. Comparison of monthly mean precipitation, standard deviation, coefficient-of-variation, 90th percentile precipitation, probability of wet-days, and wet-days intensity between the observations, raw CanRCM4, and bias-corrected (using four methods) CanRCM4 datasets during a period of 1964–1993.

Furthermore, from the view point of time-series-based statistics, the R^2 value calculated for the raw dataset was rather poor (0.04), which might have been a result of the coarse resolution of the

CanRCM4 (25 km × 25 km). After applying bias-correction methods, significant improvements on R^2 values were obtained, being close to the perfect value of 1.0. Moreover, PBIAS values improved significantly (from 10.80% to <0.69%). Similar improvements were observed from other statistics, such as NSE and MAE.

Observing the temporal trend and analyzing the goodness-of-fit statistics, it was found that while the LS method effectively removed the bias in mean precipitation, it failed to improve other statistics such as the standard deviation and probability of wet-days. The LOCI and DM methods, on the other hand, could significantly improve the mean, the probability of wet-days, and the intensity of wet-days. However, these methods over-adjusted variability statistics such as standard deviation. A similar result was observed for the coefficient-of-variation, too. In contrast, the PT method could significantly improve the variability statistics while it was found to be rather poor in adjusting the probability as well as intensity of wet-days. Hence, from the results, it could be stated that, except for the LS, other three methods (LOCI, PT and DM) have shown their own advantages to bias-correcting precipitation time series. The results further highlighted the need of bias-correcting raw RCM or GCM datasets before using them for any climate change impact assessments. Contrasting the results for the probability of wet-days and wet-days intensity indicated that the raw CanRCM4 dataset tended to have a more frequent number of wet-days of lower intensities compared to the observations. Interestingly, raw CanRCM4 data showed significantly lower wet-days intensities of precipitation, especially for the summer months (June to August), which are of higher importance to erosion and sediment transport, and nutrients exports to receiving waters.

As stated in Section 2.6, we also used GCDC stations to validate the accuracy of the bias-correction methods on precipitation and temperature. Results showed comparable accuracy to that obtained for the Glen Allen station (Table 2, Figure 3). As an illustration, both frequency- and time-series-based results (Tables S1 and S2) obtained for a GCDC station located near to the outlet of the Grand River basin showed comparable accuracy to those obtained for the Glen Allen (located in the upstream part of the basin). This also validated the need to bias-correct the raw CanRCM4 data using different methods.

3.2.2. Temperature

Since the results of different bias-correction methods for minimum temperature time series were similar to that of the maximum temperature, we presented the results of maximum temperature analysis, for clarity purposes. Table 3 shows the frequency- and time-series-based goodness-of-fit statistics, while Figure 4 presents graphical comparison between observed, and raw, as well as bias-corrected, daily maximum temperature data.

Table 3. Frequency- (daily) and time-series- (monthly) based statistics for maximum temperature of the observations, raw CanRCM4, and bias-corrected (using three methods) CanRCM4 datasets during the period of 1964–1993.

Statistics	Obs.	Raw	LS	VS	DM
Frequency based					
Mean (°C)	10.83	14.47	10.83	10.83	10.83
Median (°C)	11.1	13.92	10.71	10.93	11.42
Standard Deviation (°C)	11.71	13.21	11.83	11.71	11.71
Coefficient of Variation	1.08	0.91	1.09	1.08	1.08
90th Percentile (°C)	26	32.49	26.77	26.08	26.01
10th Percentile (°C)	–5	–1.69	–4.12	–4.83	–4.37
Time-series based					
Coefficient of Determination - R^2	-	0.92	0.93	0.94	0.93
Percentage Bias - PBIAS (%)	-	–33.84	–0.02	–0.01	–0.01
Nash-Sutcliffe Efficiency - NSE	-	0.84	0.93	0.94	0.93
Mean Absolute Error - MAE (°C)	-	4.23	2.31	2.05	2.2

LS: Linear Scaling; VS: Variance Scaling; DM: Distribution Mapping

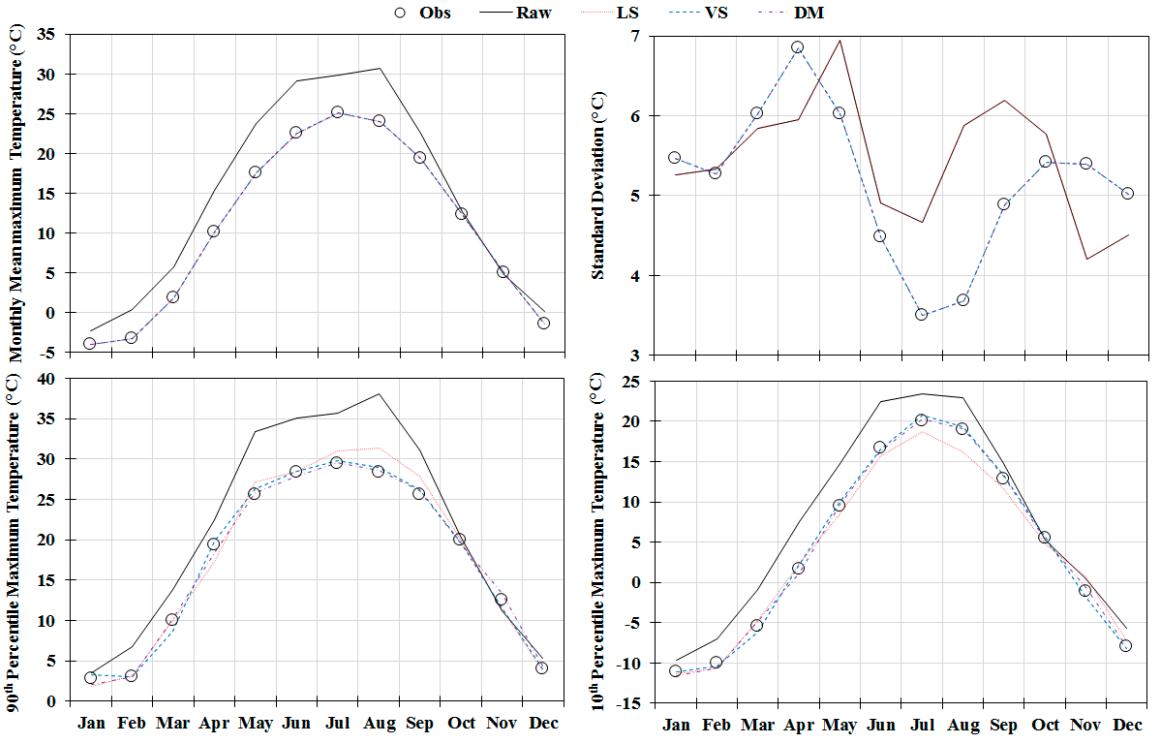

Figure 4. Comparison of monthly mean, standard deviation, 90th percentile, 10th percentile of maximum temperature between the observations, raw CanRCM4 and bias-corrected (three methods) CanRCM4 datasets during the period of 1964–1993.

As illustrated above, the raw CanRCM4 dataset tended to significantly overestimate mean maximum temperatures for all months, except for the late autumn season (October and November) months, leading to an overall overestimation (14.47 °C), compared to the observations (10.83 °C). However, after applying different bias-correction methods on the raw CanRCM4 dataset, this problem was effectively resolved. Raw CanRCM4-based standard deviations (SD) tended to overestimate the SDs for the months of May to October: however, the contrary was observed in other months, leading to an overall overestimation (13.92 °C), compared to the observations (11.71 °C). After applying different bias-correction methods, the SDs calculated for the VS and DM methods were in close agreement, while the SD for LS method was slightly higher (11.83 °C). Moreover, a similar trend to that observed in the mean temperature has been observed for the 90th percentile and 10th percentiles of maximum temperature—a serious overestimation by the raw CanRCM4 dataset and a near perfect match after applying bias-correction methods. However, the coefficient-of-variation (CV) calculated for the raw CanRCM4 dataset was slightly lower (0.91 °C) than that of the observations (1.08 °C). The CVs calculated for bias-corrected CanRCM4 dataset were in close agreement with those of the observations.

Furthermore, from the viewpoint of time-series-based statistics, unlike that observed for precipitation, R^2 values for the raw and bias-corrected CanRCM4 datasets were fairly comparable (0.92 to 0.94). However, PBIAS for the raw CanRCM4 dataset (−33.84%) improved significantly after applying any of the bias-correction methods (−0.01% to 0.02%). A similar trend was observed for NSE and MAE.

As obtained for precipitation, both frequency- and time-series-based results for temperature (Table S2) also showed comparable results for the chosen GCDC station to that of the Glen Allen station. This further highlights the need to apply different bias-correction methods to the raw CanRCM4 data.

From the analyses, it was found that all bias-correction methods significantly improved the raw CanRCM4 maximum temperature dataset. The biases in the mean temperature calculated for the three bias-correction methods were all in close agreement. Overall, with the exception of mean temperature,

the VS- and DM-based bias-corrected CanRCM4 datasets resulted in slightly better frequency-based statistics in comparison to the LS-based bias-corrected CanRCM4 dataset. The VS-based bias-corrected CanRCM4 dataset resulted in slightly better time-series-based statistics than those calculated for other methods. From the evaluation of the raw and bias-corrected CanRCM4 datasets for maximum temperatures, the need of bias-correction for temperature dataset was further highlighted.

3.2.3. Streamflow

Table 4 presents time-series-based goodness-of-fit statistics calculated for different combinations of bias-correction methods for precipitation and temperature in simulating streamflow at four gauging stations.

Table 4. Goodness-of-fit statistics for streamflow simulation in baseline, raw, and 12 different combinations of bias-correction methods for temperature and precipitation.

Simulations/ Combinations	Grand River near Marsville			Grand River at Brantford			Thames River at Ingersoll			Thames River at Thamesville		
	R^2	PBIAS (%)	NSE	R^2	PBIAS (%)	NSE	R^2	PBIAS (%)	NSE	R^2	PBIAS (%)	NSE
Baseline	0.93	–10.9	0.91	0.94	–4.25	0.86	0.81	6.42	0.79	0.98	1.63	0.97
Raw	0.61	11.49	0.22	0.68	4.77	0.64	0.69	–2.01	0.59	0.83	–4.01	0.81
P(LS) + T(LS)	0.68	–44	0.46	0.77	–36.66	0.52	0.62	–36.69	0.3	0.78	–29.81	0.52
P(LS) + T(VS)	0.67	–43.36	0.4	0.76	–36.6	0.51	0.62	–35.99	0.25	0.83	–22.07	0.56
P(LS) + T(DM)	0.67	–43.24	0.43	0.77	–36.78	0.52	0.6	–36.72	0.28	0.76	–29.57	0.5
P(LOCI) + T(LS)	0.73	–26.7	0.6	0.83	–18.86	0.73	0.67	–19.95	0.48	0.86	–15.35	0.75
P(LOCI) + T(VS)	0.71	–25.91	0.54	0.81	–18.62	0.72	0.67	–19.03	0.43	0.86	–14.68	0.73
P(LOCI) + T(DM)	0.73	–25.95	0.58	0.83	–18.93	0.73	0.65	–19.97	0.46	0.85	–15.16	0.73
P(PT) + T(LS)	0.7	–52.83	0.44	0.77	–43.77	0.49	0.72	–41.55	0.43	0.78	–33.81	0.56
P(PT) + T(VS)	0.69	–52.39	0.39	0.77	–43.92	0.48	0.74	–41.11	0.41	0.77	–33.37	0.54
P(PT) + T(DM)	0.7	–52.23	0.42	0.77	–43.97	0.49	0.72	–41.63	0.42	0.76	–33.75	0.54
P(DM) + T(LS)	0.78	–14	0.72	0.84	–6.2	0.83	0.63	–7.04	0.57	0.92	–4.95	0.9
P(DM) + T(VS)	0.78	-13.45	0.69	0.85	–6.19	0.83	0.64	–6.13	0.56	0.92	–4.34	0.9
P(DM) + T(DM)	0.79	–13.44	0.72	0.85	–6.48	0.84	0.63	–7.07	0.58	0.91	–4.9	0.89

P: Precipitation; T: Temperature
LS: Linear Scaling; VS: Variance Scaling; DM: Distribution Map; LOCI: Local Intensity Scaling; PT: Power Transformation

As expected, the baseline scenario has resulted in the best goodness-of-fit statistics, as we used a calibrated parameter set and an observed meteorological (GCDC, Figure 1) data set for this analysis. Raw CanRCM4-based streamflow resulted in systematically lower values of all statistics at all four stations. For instance, at Grand River near Marsville, the R^2 value decreased to 0.61, compared to 0.93 calculated for the baseline; and the NSE value decreased to 0.22, compared to 0.91, calculated for the baseline. The values of goodness-of-fit statistics increased for all bias-correction methods and their combinations, when compared to those that were calculated for raw CanRCM4, which further highlights the need of bias-correction on the raw future climate dataset. Furthermore, for our case, the choice of a particular bias-correction method for temperature did not seem to affect the streamflow simulation results profoundly. For instance, the goodness-of-fit statistics for combinations P(LS) + T(LS) and P(LS) + T(VS) were fairly comparable across all stations. However, the choice of a particular bias-correction method for precipitation tended to affect streamflow simulation results profoundly. As illustrated, the goodness-of-fit statistics for the combination of P(LOCI) + T(LS) were consistently better than those obtained for the combination of P(LS) + T(LS) across all stations. Our findings suggest that the selection of a particular bias-correction method for precipitation would exert greater control than that for temperature, and highlights the need for a proper bias-correction method for raw CanRCM4 precipitation data. Overall, after a systematic evaluation of all the combinations was completed, it was evident that the combination of P(DM) + T(DM) performed the best, and the precipitation and temperature dataset obtained after respective bias-corrections were used for further analysis.

3.3. Streamflow Results in Future Periods

Figures 5 and 6 shows the spatiotemporal variation of mean monthly changes in precipitation (%) and mean temperature (°C) at the sub-basin spatial scale. Table 5 shows the basin-wide changes in precipitation (%), mean temperature (°C), green water flow (evapotranspiration—ET, %) and green water storage (soil water, %) in a monthly time interval. Here, we opted to use the terminologies that are consistent with the so-called 'green and blue water paradigm', as advocated by Falkenmark and Rockström [53]. It should be noted that we did not validate either the green water flow or green water storage due to the unavailability of the data. However, because we achieved "very good" streamflow results at multiple locations, it is fair to assume that these two important components (green water flow or green water storage) were well simulated when using a physically-based model such as the SWAT.

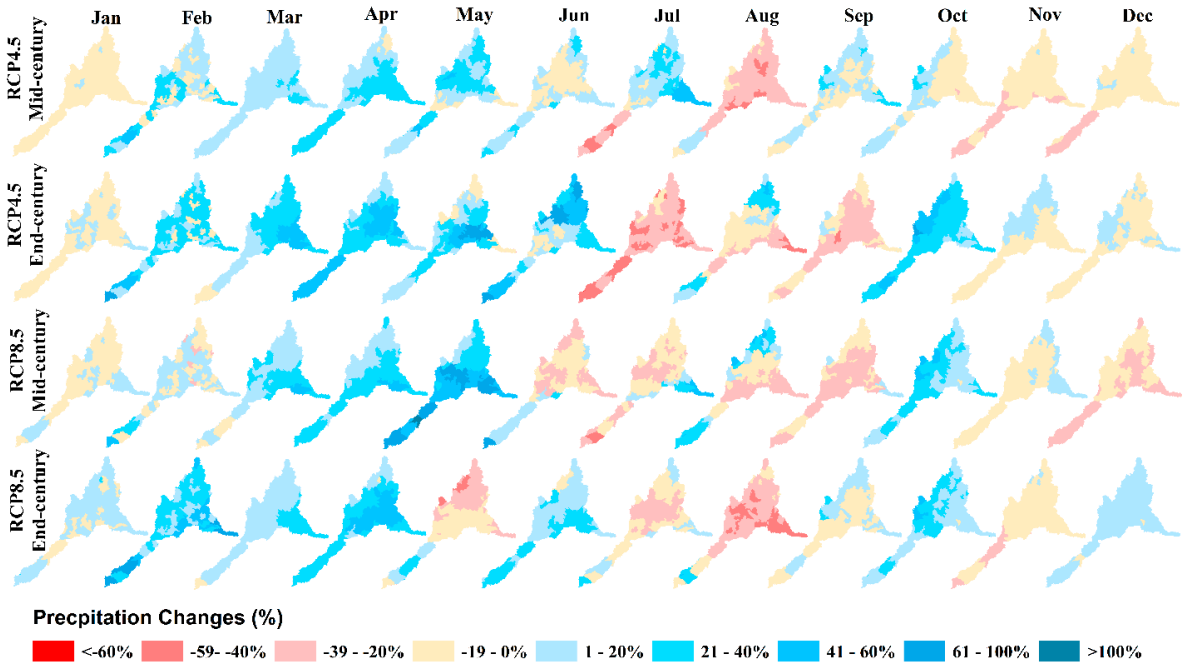

Figure 5. Changes in precipitation (%) in different future periods and for different emission scenarios, compared to the base period.

On average, precipitation was projected to increase in the winter and spring months, and to decrease in the summer and autumn months. The increases and decreases tended to be more extreme for the higher emission scenario (RCP8.5), and for the end-of-century period (2083–2093). The highest increase in precipitation was expected in the month of May, and during the mid-century period for the RCP8.5 scenario (+55%) while a decrease of −11% was expected in the same month for the same emission scenario, but in the end-of-century period. This shows marked heterogeneity in the projected precipitation changes as per the emission scenarios and in different future periods. The summer precipitation, which was of particular importance for crop growth, as most of the crops would be in their most critical stage (e.g., flowering), was expected to decrease, on average—the highest decreases were in the month of August (−6% to −27%). Interestingly, for both emission scenarios and in both future periods, spring (March-May) precipitation was projected to increase, on average (up to +55%). Our results were comparable to those reported in similar Canadian watersheds [26,54–56]; including by Rahman et al. [57] in the Ruscom River basin, and in the watersheds around the Great Lake basins, such as those reported by Cousino et al. [58] and Culbertson et al. [12] in the Maumee River basin, by Bosch et al. [11] in four basins draining to Lake Erie from the USA, by Li et al. [14] in the Grand River basin, and by Samantha et al. [59] in the Western Lake Erie basin, among others.

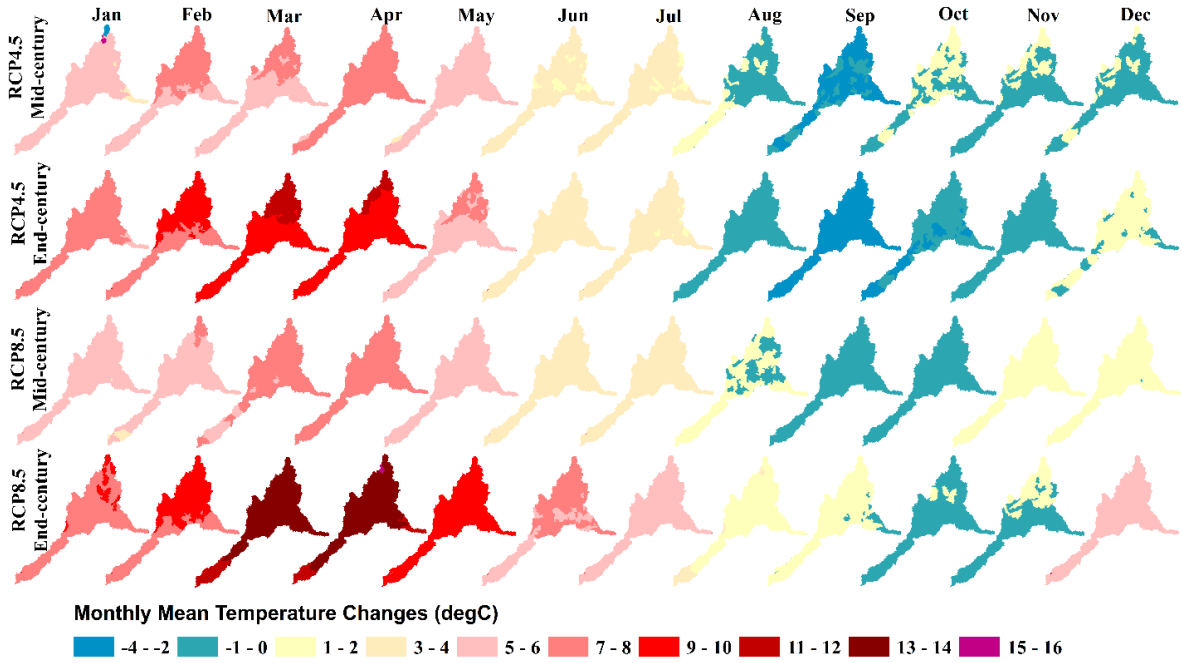

Figure 6. Changes in mean air temperature (°C) in different future periods and for different emission scenarios, compared to the base period.

Table 5. Projected changes in basin-wide average precipitation, mean temperature, green water flow (evapotranspiration–ET) and green water storage (soil water) in two emission scenarios and during two future periods, compared to the base period.

Variables	Emission Scenarios/Periods	Jan	Feb	Mar	Apr	May	Jun	Jul	Aug	Sep	Oct	Nov	Dec
Precipitation Changes (%)	RCP4.5 Mid-century	–12	16	11	23	11	6	–5	–27	0	2	–19	–15
	RCP8.5 Mid-century	–1	7	15	27	55	4	–10	–6	–21	21	–3	–23
	RCP4.5 End-century	–6	26	18	32	19	31	–40	–12	–22	31	–7	–5
	RCP8.5 End-century	3	38	8	27	–11	18	-1	–27	-2	21	–16	6
Average Temperature Changes (°C)	RCP4.5 Mid-century	4.5	5.8	5.6	6.5	4.5	2.4	2.5	0.2	–2.0	–0.1	–0.3	–0.1
	RCP8.5 Mid-century	4.6	4.7	6.3	6.5	5.2	3.3	3.0	0.4	–0.7	–0.8	0.5	0.8
	RCP4.5 End-century	6.7	7.7	9.4	9.2	5.9	3.1	2.9	–0.7	–2.8	–1.9	–0.8	0.3
	RCP8.5 End-century	7.8	7.9	12.4	12.5	8.8	6.1	5.6	2.0	0.4	–0.4	–0.2	5.6
Green Water Flow Changes (%)	RCP4.5 Mid-century	125	128	58	39	38	9	–12	–26	–23	–8	15	10
	RCP8.5 Mid-century	123	119	55	36	42	7	–11	–23	–12	–12	18	19
	RCP4.5 End-century	170	157	73	54	51	5	–22	–39	–23	–12	10	15
	RCP8.5 End-century	188	173	88	70	53	1	–16	–48	–34	–15	9	56
Green Water Storage Changes (%)	RCP4.5 Mid-century	–15	–21	–10	–3	–22	–35	–37	–33	–4	5	–4	1
	RCP8.5 Mid-century	–15	–19	–12	–2	–21	–35	–40	–12	–12	9	0	–9
	RCP4.5 End-century	–19	–23	–15	–3	–34	–30	–52	–9	–9	14	–1	–1
	RCP8.5 End-century	–20	–22	–20	–19	–56	–50	–37	–6	12	12	–4	–9

As observed for precipitation, there existed marked spatial and temporal variabilities in the projected mean temperature. In the spatial scale, the changes in the upper parts of the basin were slightly more extreme than those in the lower parts of the basin. Moreover, the changes were more extreme for the RCP 8.5 emission scenario and during the end-of-century period. During the winter and spring months, the increases were the highest (up to +12.5 °C, in April for the RCP 8.5 during the end-of-century period). The increasing trend in temperature was expected to continue until July. The temperature, however, was expected to decrease in the autumn months, contrary to most of the studies conducted in surrounding basins [11,12,14,57,58].

With the increasing trend in temperatures during the winter season (up to +7.9 °C), the green water flow (evapotranspiration—ET) increased significantly (up to +188%), thereby decreasing the green water storage (soil moisture, up to −23%), even if the winter season was projected to receive more precipitation, on average (up to +38%). These increases in winter precipitation could have the so-called 'rain-on-snow' (ROS) effects which have the potential to accelerate snowmelt, thereby decreasing snowpack and lowering the soil water content in spring [60], which was what we observed—decreases of up to −56% on green water storage in the spring season. These projected decreases in green water storage could affect crop sowing and plantation dates. In the summer season, projected decreases in precipitation (up to −40%) and projected increases in temperature (up to +6.1 °C) seemed to have offsetting effects, as green water flow was expected to decrease, on average. This could be attributed to projected decreases in green water storage (up to −52%), which consequently restricted the ability of crops to allow increased green water flow as a result of projected increases in summer temperature. Such consistent decreases of green water storage (up to −52%) during the summer period, a crucial period of time for crop growth and development, would have serious implications on the crop yield, as crops might experience water-stress conditions. Consequently, farmers may have to irrigate their crop field in order to optimize the crop yield. In the autumn season, green water flow decreases (up to −34%) as a result of projected decreases (on average) in temperature (up to −2.8 °C), thereby increasing green water storage (up to +14%).

Figure 7 shows the monthly streamflow dynamics in the baseline and future periods at four gauging stations. In general, there was a clear shift of spring snowmelt toward the late winter months or the early spring months. Additionally, decreases in the average summer streamflow were noted, which corresponded to the observations made in similar cold climate regions [26,54–56,61,62] including those in the Great Lake basin [11–14,57,58].

In the Grand River near Marsville, mean monthly streamflow was projected to increase in mid- and late-winter months (January and February), late-spring (May), and early- and mid-summer months (Figure 7 & Table S4). Furthermore, there was also a clear shift in the occurrence of spring snowmelt to earlier months (February). This particular gauging station is located in the upstream part of the Grand River basin (Figure 1), where the changes in winter temperatures clearly showed higher increases in comparison to other parts of the basin (Figure 6), thereby significantly increasing green water flow (evapotranspiration—ET, Figure S4). Such elevated winter temperatures compounded by projected increases in late-winter (February) precipitation in this region (Figure 5), results in increases (+20 to +83%, Table S4) in February streamflow. As a consequence, streamflow during the early spring months (March and April) was projected to decrease substantially (−39% to −51% during March, and −60% to −72% during April), despite projected increases in precipitation during these months, since less snowpack was available for melting, and thus soil moisture level was depleted (Figure S5, Table S4). Interestingly, during the summer months, changes in precipitation (−37% to +54%, Figure 5 & Table 5) had been reflected in the streamflow dynamics (−77% to +170%). Such high variability in the projected changes of summer streamflow poses additional challenges to water managers and planners. During the autumn months, as similarly observed with summer streamflow, the magnitude of changes varied profoundly as per RCPs and future periods. For instance, for RCP8.5 in August, streamflow was projected to increase by +119% during the mid-century period, but was expected to decrease by –57% during the end-of-century period (Figure 7 & Table S4). When analyzing the spatial variability of projected changes in precipitation and temperature at upstream regions of the Grand River basin, it was clear that the slightest of changes in these climate variables could translate into amplified changes on streamflow.

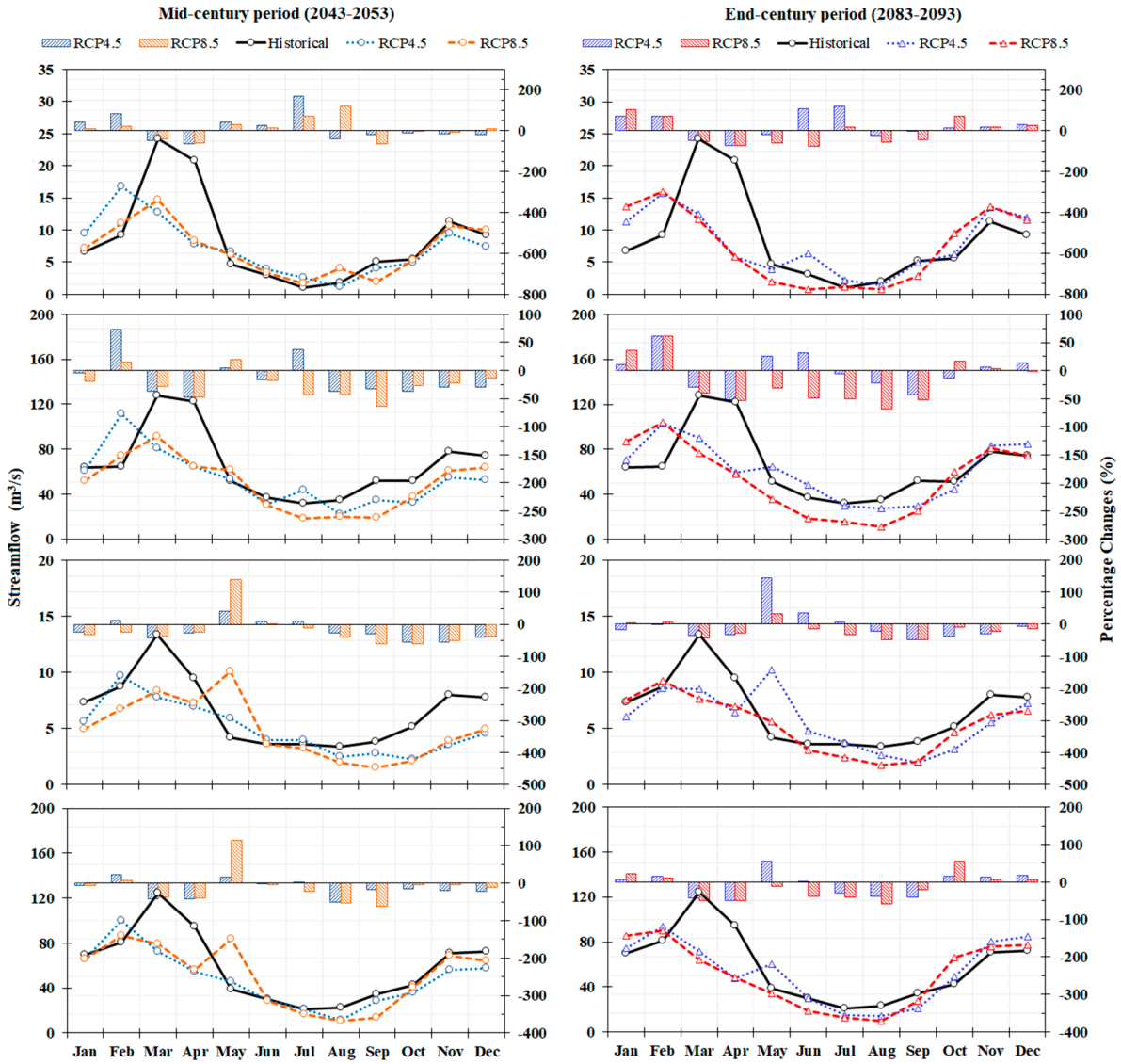

Figure 7. Time series plot of mean monthly streamflow in the baseline and future periods (for different future periods and emission scenarios) at (**a**) Grand River near Marsville, (**b**) Grand River at Brantford, (**c**) Thames River at Ingersoll, and (**d**) Thames River at Thamesville. Also shown: the percentage of change in streamflow as bars.

In the Grand River at Brantford (the downstream station, Figure 1), changes in streamflow had generally followed the trend observed in Marshville (the upstream station, Figure 1) for the winter and spring months—a clear shift in the occurrence of spring snowmelt to an earlier month (February) and decreases in early spring (March and April) streamflow. In spring months, the importance of antecedent soil moisture level and of temperature exerting greater control than precipitation, were clearly highlighted in such cold climate region watersheds. For instance, in March, the precipitation in RCP8.5 during the end-of-century period was projected to increase by 17% (Table S4); however, streamflow was shown to decrease (−40%, Table S4). This was due to the fact that temperature was expected to increase significantly (+13.1 °C, Table S3), thereby increasing green water flow (+130%). Such decreases in streamflow were also a result of lower green water storage in the previous month (−20%, Table S3). However, summer streamflow at Brantford was projected to decrease (up to −68%), corresponding with findings of Li et al. [14] in the same river basin. While the differences in the projected changes of streamflow between RCP 4.5 and RCP8.5 during the mid-century period were

fairly comparable (with the exception of July), contrasting results were evident, especially during the summer months in the end-of-century period (Figure 7). This could be related to the differences in the projected increases in temperature. During the end-of-century period, even though the magnitudes of changes in precipitation were fairly comparable (Figure 5), changes in temperature were significantly higher for RCP8.5 (Figure 6, Table S3), thereby increasing the green water flow (Figure S4, Table S3) and decreasing soil water storage (Figure S5, Table S3). Similarly, autumn streamflow, on average, was projected to decrease (up to −64%), reflecting the average projected decreases in precipitation. It should be noted that autumn temperature was expected to decrease, implying that precipitation exerts greater control on streamflow dynamics than temperature, in autumn months.

In the Thames River at Ingersoll (with the exception of RCP8.5 during end-of-century period), mid-winter (January) streamflow was projected to decrease (up to −33%). Furthermore, for RCP8.5 during mid-century and RCP 4.5 during end-of-century, peak streamflow was projected to occur in May, with increases of +140% and +144%, respectively (Figure 7 & Table S4). Such significant increases were driven by projected increases of localized precipitation in sub-basins draining to this station (increases up to 55% and 26%, respectively, which were significantly higher than other locations, Table S3). This highlights the effects that localized changes in climatic variables can have in smaller watersheds, with a short time of concentration. As also observed in two stations of the Grand River basin, streamflow in the early spring months (March and April) was projected to decrease consistently (up to −43%), irrespective of the emission scenario and the future period. Similarly, summer and autumn streamflow were also projected to decrease, on average, which was in line with the conclusions of Culbertson et al. and Verma et al. [12,13] in the Maumee River basin, Cherkauer and Sinha [9] in six watersheds of Lake Michigan, and Chien et al. [63] in four watersheds of midwestern US.

In Thamesville, the downstream station of the Thames River basin (Figure 1), the general trends of: increases in winter streamflow, decreases in early- and mid-spring (March and April, respectively) streamflow, decreases in summer and autumn (on average) streamflow, and a clear shift of peak early-spring (March) streamflow to late-winter (February), were observed. However, significant increases in May streamflow (up to +115%, Figure 7 & Table S4) for RCP8.5 during the mid-century period and RCP4.5 during the end-of-century period (+55%) were evident at this station, as well as at the upstream station, due to projected increases in precipitation (63% and 54%, respectively, refer Table S3). Furthermore, mid- (October) and late-autumn (November) streamflow were expected to increase (up to +56%), reflecting the projected changes in precipitation.

From the analyses, it is clear that there existed marked spatial variability in the projected changes in streamflow, due to the spatial heterogeneity of precipitation and temperature changes, and of evapotranspiration and soil water storage changes. Furthermore, there existed marked differences in the streamflow changes as per the RCPs and the future periods (Figure 8). For instance, at the Grand River near Marsville, January streamflow would vary between 7.2 to 13.6 m^3/s (Figure 8). This further highlights the need to consider spatial variability and availability of water resources distribution in the future, as well as the need to consider different emission scenarios and different future periods in such climate change impact assessments. The results of this study also warranted that region-specific adaptation measures need to be placed in the Lake Erie Basin in order to lessen the impacts of climate change on the basins water resources in the future. Moreover, the need for bias-correction on the raw CanRCM data was further highlighted by the marked differences in streamflow projections, based on the raw and bias-corrected climate data (Figure 8). As we did not endeavor to present streamflow results derived by the raw climate data, we did not further elaborated on it. However, precautions should be taken when inferring the future streamflow variabilities, which were based on the raw climate data.

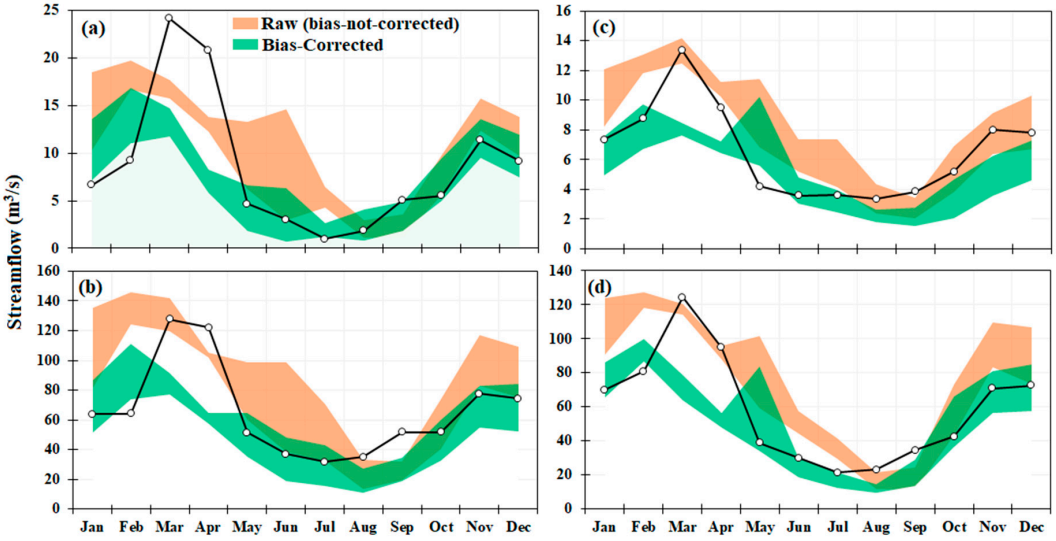

Figure 8. Time series plot of mean monthly streamflow in the baseline period (line with markers) and range (maximum and minimum, as shaded area) of streamflow in the future period (for different future periods and emission scenarios) at (**a**) the Grand River near Marsville; (**b**) the Grand River at Brantford; (**c**) the Thames River at Ingersoll; and (**d**) the Thames River at Thamesville, with raw (bias-not-corrected) and bias-corrected datasets.

4. Conclusions

This work demonstrates the need for the application and evaluation of different bias-correction methods (and their combinations) before forcing climatic data into a calibrated and validated SWAT model for climate change impact assessment, considering that the bias-correction methods significantly improved the raw climatic data. Furthermore, the advantages of analyzing climate change impact on different spatial and temporal scales, considering different components of the hydrological cycles, were illustrated. The severity of the impact differed for each of the components. As an example, streamflow was projected to decrease in all seasons (spring: −33%, summer: −23% and autumn: −15%), with the exception of winter (+11%), as a response to the projected warmer (up to +14 °C) and wetter (up to +63%) climate in these two rivers of the NLE basin.

This study is first of its kind to explore the region-specific temporal variability in water resource availability. Such variability poses a considerable challenges to water planners and managers, as well as the integrated water resources management of these two river basins. We believe that the availability of such a modelling tool, and the knowledge of climate-induced hydrological altercations could be helpful in understanding the distribution and availability of water resources in the future, and would aid in the formulation of plausible management options in the view of mitigating any ill effects on the health of Lake Erie.

Supplementary Materials: The following are available online at http://www.mdpi.com/2071-1050/10/8/2897/s1, Figure S1: Land use map of the study area. Land use names are presented as in SWAT database, Figure S2: Different soil types in the study area. Soil names are presented as in the Ontario Ministry of Agriculture, Food and Rural Affairs, Figure S3: The slope map of the study area, Figure S4: Changes in green water flow (evapotranspiration—ET) in different future periods and for different emission scenarios, compared to the base period, Figure S5: Changes in green water storage (soil water) in different future periods and for different emission scenarios, compared to base period, Table S1: Frequency- (daily) and time-series- (monthly) based statistics for precipitation of observation, raw CanRCM4, and bias-corrected (using four methods) CanRCM4 datasets during a period of 1980–1993 at a pixel near the outlet of the Grand river basin, Table S2: Frequency- (daily) and time series- (monthly) based statistics for the maximum temperature of observation, raw CanRCM4, and bias-corrected (using three methods) CanRCM4 datasets during a period of 1980–1993 at a pixel near the outlet of the Grand river basin, Table S3: Projected future changes in mean monthly precipitation, mean temperature, evapotranspiration, and soil water storage, averaged for the sub-basins upstream of four stations, Table S4: Projected future changes in mean monthly streamflow at four stations.

Author Contributions: Conceptualization, P.D. and R.R.; Methodology, B.Z., P.D. and R.R.; Validation, B.Z., N.K.S., P.D., R.S., B.K., and J.H., Formal Analysis, B.Z., N.K.S., P.D., and R.S.; Investigation, B.Z., N.K.S., P.D., and R.S.; Data Curation, B.Z. and P.D.; Writing—Original Draft Preparation, B.Z., N.K.S., P.D., and R.S.; Writing—Review & Editing, B.Z., N.K.S., P.D., and R.S.; Visualization, B.Z., N.K.S., P.D., and R.S.; Supervision, P.D. and R.R.

Funding: The funding for this study is provided by the NSERC-Discovery Grant.

Acknowledgments: The funding for this study is provided by the NSERC-Discovery Grant. We would like to thank Ms. Melissa Hardy for proofreading the manuscript.

Conflicts of Interest: The authors declare no conflict of interest.

References

1. Sanderson, M. The great-lakes—An environmental atlas and resource book—Environment-canada-us-epa-brock-university-northwestern-university. *Prof. Geogr.* **1988**, *40*, 250–251.
2. Makarewicz, J.C.; Bertram, P. Evidence for the restoration of the lake erie ecosystem—Water-quality, oxygen levels, and pelagic function appear to be improving. *Bioscience* **1991**, *41*, 216–223. [CrossRef]
3. Paerl, H.W.; Hall, N.S.; Calandrino, E.S. Controlling harmful cyanobacterial blooms in a world experiencing anthropogenic and climatic-induced change. *Sci. Total Environ.* **2011**, *409*, 1739–1745. [CrossRef] [PubMed]
4. Michalak, A.M.; Anderson, E.J.; Beletsky, D.; Boland, S.; Bosch, N.S.; Bridgeman, T.B.; Chaffin, J.D.; Cho, K.; Confesor, R.; Daloglu, I.; et al. Record-setting algal bloom in lake erie caused by agricultural and meteorological trends consistent with expected future conditions. *Proc. Natl. Acad. Sci. USA* **2013**, *110*, 6448–6452. [CrossRef] [PubMed]
5. Smith, D.; King, K.; Williams, M. What is causing the harmful algal blooms in lake erie? *J. Soil Water Conserv.* **2015**, *70*, 27–29. [CrossRef]
6. Mortsch, L.D.; Quinn, F.H. Climate change scenarios for great lakes basin ecosystem studies. *Limnol. Oceanogr.* **1996**, *41*, 903–911. [CrossRef]
7. Mekis, E.; Hogg, W.D. Rehabilitation and analysis of canadian daily precipitation time series. *Atmosphere-Ocean* **1999**, *37*, 53–85. [CrossRef]
8. Uniyal, B.; Jha, M.; Verma, A. Assessing climate change impact on water balance components of a river basin using swat model. *Water Resour. Manag.* **2015**, *29*, 4767–4785. [CrossRef]
9. Cherkauer, K.A.; Sinha, T. Hydrologic impacts of projected future climate change in the lake michigan region. *J. Great Lakes Res.* **2010**, *36*, 33–50. [CrossRef]
10. Newham, L.T.H.; Letcher, R.A.; Jakeman, A.J.; Kobayashi, T. A framework for integrated hydrologic, sediment and nutrient export modelling for catchment-scale management. *Environ. Model. Softw.* **2004**, *19*, 1029–1038. [CrossRef]
11. Bosch, N.S.; Evans, M.A.; Scavia, D.; Allan, J.D. Interacting effects of climate change and agricultural bmps on nutrient runoff entering lake erie. *J. Great Lakes Res.* **2014**, *40*, 581–589. [CrossRef]
12. Culbertson, A.M.; Martin, J.F.; Aloysius, N.; Ludsin, S.A. Anticipated impacts of climate change on 21st century maumee river discharge and nutrient loads. *J. Great Lakes Res.* **2016**, *42*, 1332–1342. [CrossRef]
13. Verma, S.; Bhattarai, R.; Bosch Nathan, S.; Cooke Richard, C.; Kalita Prasanta, K.; Markus, M. Climate change impacts on flow, sediment and nutrient export in a great lakes watershed using swat. *CLEAN—Soil Air Water* **2015**, *43*, 1464–1474. [CrossRef]
14. Li, Z.; Huang, G.; Wang, X.; Han, J.; Fan, Y. Impacts of future climate change on river discharge based on hydrological inference: A case study of the grand river watershed in Ontario, Canada. *Sci. Total Environ.* **2016**, *548–549*, 198–210. [CrossRef] [PubMed]
15. Arnold, J.G.; Srinivasan, R.; Muttiah, R.S.; Williams, J.R. Large area hydrologic modeling and assessment part I: Model development. *J. Am. Water Resour. Assoc.* **1998**, *34*, 73–89. [CrossRef]
16. Scinocca, J.F.; Kharin, V.V.; Jiao, Y.; Qian, M.W.; Lazare, M.; Solheim, L.; Flato, G.M.; Biner, S.; Desgagne, M.; Dugas, B. Coordinated global and regional climate modeling. *J. Clim.* **2016**, *29*, 17–35. [CrossRef]
17. Rathjens, H.; Bieger, B.; Srinivasan, S.; Chaubey, I.; Arnold, J.G. CMhyd User Manual. Available online: http://swat.tamu.edu/software/cmhyd/ (accessed on 20 February 2018).
18. Intergovernmental Panel on Climate Change. *Climate Change 2014: Synthesis Report. Contribution of Working Groups I, II and III to the Fifth Assessment Report of the Intergovernmental Panel on Climate Change*; IPCC: Geneva, Switzerland, 2014; p. 151.
19. *Daily 10 km Gridded Climate Dataset: 1961–2003,* version 1.0; computer file; Agriculture and Agri-Food Canada (AAFC): Ottawa, ON, Canada, 2007.

20. *Grand River Watershed Characterization Report*; Lake Erie Source Protection Region Technical Team: Cambridge, ON, Canada, 2008.
21. Farwell, J.; Boyd, D.; Ryan, T. Making watersheds more resilient to climate change: A response in the grand river watershed, Ontario Canada. In Proceedings of the 11th Annual River symposium, Brisbane, Australia, 18–20 September 2008.
22. Goyal, M.K.; Burn, D.H.; Ojha, C.S.P. Evaluation of machine learning tools as a statistical downscaling tool: Temperatures projections for multi-stations for thames river basin, Canada. *Theor. Appl. Climatol.* **2012**, *108*, 519–534. [CrossRef]
23. Prodanovic, P.; Simonovic, S.P. Inverse Flood Risk Modelling of the Upper Thames River Basin. Water Resources Research Report. Available online: https://ir.Lib.Uwo.Ca/wrrr/12 (accessed on 20 February 2018).
24. Arnold, J.G.; Moriasi, D.N.; Gassman, P.W.; Abbaspour, K.C.; White, M.J.; Srinivasan, R.; Santhi, C.; Harmel, R.D.; van Griensven, A.; Van Liew, M.W.; et al. Swat: Model use, calibration, and validation. *Trans. ASABE* **2012**, *55*, 1491–1508. [CrossRef]
25. Shrestha, N.K.; Du, X.; Wang, J. Assessing climate change impacts on fresh water resources of the athabasca river basin, Canada. *Sci. Total Environ.* **2017**, *601–602*, 425–440. [CrossRef] [PubMed]
26. Shrestha, N.K.; Wang, J. Predicting sediment yield and transport dynamics of a cold climate region watershed in changing climate. *Sci. Total Environ.* **2018**, *625*, 1030–1045. [CrossRef] [PubMed]
27. Ahl, R.S.; Woods, S.W.; Zuuring, H.R. Hydrologic calibration and validation of swat in a snow-dominated rocky mountain watershed, montana, U.S.A. 1. *JAWRA J. Am. Water Resour. Assoc.* **2008**, *44*, 1411–1430. [CrossRef]
28. Grusson, Y.; Sun, X.; Gascoin, S.; Sauvage, S.; Raghavan, S.; Anctil, F.; Sáchez-Pérez, J.-M. Assessing the capability of the swat model to simulate snow, snow melt and streamflow dynamics over an alpine watershed. *J. Hydrol.* **2015**, *531*, 574–588. [CrossRef]
29. Faramarzi, M.; Srinivasan, R.; Iravani, M.; Bladon, K.D.; Abbaspour, K.C.; Zehnder, A.J.B.; Goss, G.G. Setting up a hydrological model of alberta: Data discrimination analyses prior to calibration. *Environ. Model. Softw.* **2015**, *74*, 48–65. [CrossRef]
30. Troin, M.; Caya, D. Evaluating the swat's snow hydrology over a northern quebec watershed. *Hydrol. Process.* **2014**, *28*, 1858–1873. [CrossRef]
31. Malagò, A.; Pagliero, L.; Bouraoui, F.; Franchini, M. Comparing calibrated parameter sets of the swat model for the scandinavian and iberian peninsulas. *Hydrol. Sci. J.* **2015**, *60*, 949–967. [CrossRef]
32. Winchell, M.; Srinivasan, R.; Luzio, M.D. *Arcswat Interface for Swat2009 User's Guide*; Soil and Water Research Laboratory—Agricultural Research Service: Blackland, TX, USA, 2010.
33. *Provincial Digital Elevation Model,* version 3.0; Ontario Ministry Of Natural Resources And Forestry: Peterborough, ON, Canada, 2015.
34. Moriasi, D.N.; Gitau, M.W.; Pai, N.; Daggupati, P. Hydrologic and water quality models: Performance measures and evaluation criteria. *Trans. ASABE* **2015**, *58*, 1763–1785.
35. Nash, J.E.; Sutcliffe, J.V. River flow forecasting through conceptual models part I—A discussion of principles. *J. Hydrol.* **1970**, *10*, 282–290. [CrossRef]
36. Shrestha, N.K.; Leta, O.T.; De Fraine, B.; van Griensven, A.; Bauwens, W. Openmi-based integrated sediment transport modelling of the river zenne, Belgium. *Environ. Model. Softw.* **2013**, *47*, 193–206. [CrossRef]
37. Shrestha, N.K.; Leta, O.T.; Bauwens, W. Development of rwqm1-based integrated water quality model in openmi with application to the river zenne, belgium. *Hydrol. Sci. J.* **2017**, *62*, 774–799. [CrossRef]
38. Von Salzen, K.; Scinocca, J.F.; McFarlane, N.A.; Li, J.N.; Cole, J.N.S.; Plummer, D.; Verseghy, D.; Reader, M.C.; Ma, X.Y.; Lazare, M.; et al. The canadian fourth generation atmospheric global climate model (canam4). Part I: Representation of physical processes. *Atmos Ocean* **2013**, *51*, 104–125. [CrossRef]
39. Hawkins, E.; Sutton, R. The potential to narrow uncertainty in regional climate predictions. *Bull. Am. Meteorol. Soc.* **2009**, *90*, 1095–1108. [CrossRef]
40. Cheng, G.H.; Huang, G.H.; Dong, C.; Zhu, J.X.; Zhou, X.; Yao, Y. An evaluation of cmip5 gcm simulations over the Athabasca river basin, Canada. *River Res. Appl.* **2017**, *33*, 823–843. [CrossRef]
41. Murdock, T.Q.; Cannon, A.J.; Sobie, S.R. *Statistical Downscaling of Future Climate Projections*; Pacific Climate Impacts Consortium (PCIC): Victoria, British Columbia, Canada, 2013.
42. Shukla, R.; Khare, P.D.; Deo, R. Statistical downscaling of climate change scenarios of rainfall and temperature over indira sagar canal command area in madhya pradesh, India. In Proceedings of the2015 IEEE 14th International Conference on Machine Learning and Applications (ICMLA), Miami, FL, USA, 9–11 December 2015; pp. 313–317.

43. Lenderink, G.; Buishand, A.; van Deursen, W. Estimates of future discharges of the river rhine using two scenario methodologies: Direct versus delta approach. *Hydrol. Earth Syst. Sci.* **2007**, *11*, 1145–1159. [CrossRef]
44. Berg, P.; Feldmann, H.; Panitz, H.J. Bias correction of high resolution regional climate model data. *J. Hydrol.* **2012**, *448*, 80–92. [CrossRef]
45. Olsson, T.; Jakkila, J.; Veijalainen, N.; Backman, L.; Kaurola, J.; Vehvilainen, B. Impacts of climate change on temperature, precipitation and hydrology in finland—Studies using bias corrected regional climate model data. *Hydrol. Earth Syst. Sci.* **2015**, *19*, 3217–3238. [CrossRef]
46. Schmidli, J.; Frei, C.; Vidale, P.L. Downscaling from gc precipitation: A benchmark for dynamical and statistical downscaling methods. *Int. J. Climatol.* **2006**, *26*, 679–689. [CrossRef]
47. Teutschbein, C.; Seibert, J. Bias correction of regional climate model simulations for hydrological climate-change impact studies: Review and evaluation of different methods. *J. Hydrol.* **2012**, *456*, 12–29. [CrossRef]
48. Fang, G.H.; Yang, J.; Chen, Y.N.; Zammit, C. Comparing bias correction methods in downscaling meteorological variables for a hydrologic impact study in an arid area in china. *Hydrol. Earth Syst. Sci.* **2015**, *19*, 2547–2559. [CrossRef]
49. Leander, R.; Buishand, T.A.; van den Hurk, B.J.J.M.; de Wit, M.J.M. Estimated changes in flood quantiles of the river meuse from resampling of regional climate model output. *J. Hydrol.* **2008**, *351*, 331–343. [CrossRef]
50. Terink, W.; Hurkmans, R.T.W.L.; Torfs, P.J.J.F.; Uijlenhoet, R. Evaluation of a bias correction method applied to downscaled precipitation and temperature reanalysis data for the rhine basin. *Hydrol. Earth Syst. Sci.* **2010**, *14*, 687–703. [CrossRef]
51. Mbaye, M.L.; Haensler, A.; Hagemann, S.; Gaye, A.T.; Moseley, C.; Afouda, A. Impact of statistical bias correction on the projected climate change signals of the regional climate model remo over the senegal river basin. *Int. J. Climatol.* **2016**, *36*, 2035–2049. [CrossRef]
52. Tschoke, G.V.; Kruk, N.S.; Queiroz, P.I.B.; Chou, S.; de Sousa, W.C. Comparison of two bias correction methods for precipitation simulated with a regional climate model. *Theor. Appl. Climatol.* **2017**, *127*, 841–852. [CrossRef]
53. Falkenmark, M.; Rockström, J. The new blue and green water paradigm: Breaking new ground for water resources planning and management. *J. Water Resour. Plan. Manag.* **2006**, *132*, 129–132. [CrossRef]
54. Eum, H.-I.; Dibike, Y.; Prowse, T. Climate-induced alteration of hydrologic indicators in the athabasca river basin, alberta, Canada. *J. Hydrol.* **2017**, *544*, 327–342. [CrossRef]
55. Toth, B.; Pietroniro, A.; Conly, F.M.; Kouwen, N. Modelling climate change impacts in the peace and athabasca catchment and delta: I—Hydrological model application. *Hydrol. Process.* **2006**, *20*, 4197–4214. [CrossRef]
56. Choi, W.; Kim, S.J.; Lee, M.; Koenig, K.; Rasmussen, P. Hydrological impacts of warmer and wetter climate in troutlake and sturgeon river basins in central canada. *Water Resour. Manag.* **2014**, *28*, 5319–5333. [CrossRef]
57. Rahman, M.; Bolisetti, T.; Balachandar, R. Effect of climate change on low-flow conditions in the ruscom river watershed, ontario. *Trans. ASABE* **2010**, *53*, 1521–1532. [CrossRef]
58. Cousino, L.K.; Becker, R.H.; Zmijewski, K.A. Modeling the effects of climate change on water, sediment, and nutrient yields from the maumee river watershed. *J. Hydrol. Reg. Stud.* **2015**, *4*, 762–775. [CrossRef]
59. Basile Samantha, J.; Rauscher Sara, A.; Steiner Allison, L. Projected precipitation changes within the great lakes and western lake erie basin: A multi-model analysis of intensity and seasonality. *Int. J. Climatol.* **2017**, *37*, 4864–4879. [CrossRef]
60. Cohen, J.; Ye, H.; Jones, J. Trends and variability in rain-on-snow events. *Geophys. Res. Lett.* **2015**, *42*, 7115–7122. [CrossRef]
61. Choi, W.; Rasmussen, P.; Moore, A.; Kim, S. Simulating streamflow response to climate scenarios in central canada using a simple statistical downscaling method. *Climate Res.* **2009**, *40*, 89–102. [CrossRef]
62. Shrestha, R.R.; Dibike, Y.B.; Prowse, T.D. Modelling of climate-induced hydrologic changes in the lake winnipeg watershed. *J. Great Lakes Res.* **2012**, *38*, 83–94. [CrossRef]
63. Chien, H.; Yeh, P.J.F.; Knouft, J.H. Modeling the potential impacts of climate change on streamflow in agricultural watersheds of the midwestern united states. *J. Hydrol.* **2013**, *491*, 73–88. [CrossRef]